analytical chemistry

pubs.acs.org/ac Article

Particle Size Distributions for Cellulose Nanocrystals Measured by Transmission Electron Microscopy: An Interlaboratory Comparison

Juris Meija, Michael Bushell, Martin Couillard, Stephanie Beck, John Bonevich, Kai Cui, Johan Foster, John Will, Douglas Fox, Whirang Cho, Markus Heidelmann, Byong Chon Park, Yun Chang Park, Lingling Ren, Li Xu, Aleksandr B. Stefaniak, Alycia K. Knepp, Ralf Theissmann, Horst Purwin, Ziqiu Wang, Natalia de Val, and Linda J. Johnston*

Cite This: *Anal. Chem.* 2020, 92, 13434–13442 Read Online

ACCESS | Metrics & More | Article Recommendations | Supporting Information

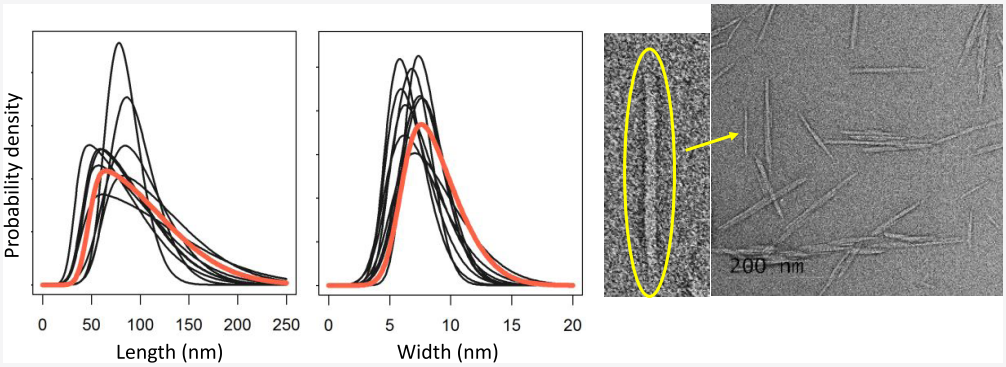

ABSTRACT: Particle size is a key parameter that must be measured to ensure reproducible production of cellulose nanocrystals (CNCs) and to achieve reliable performance metrics for specific CNC applications. Nevertheless, size measurements for CNCs are challenging due to their broad size distribution, irregular rod-shaped particles, and propensity to aggregate and agglomerate. We report an interlaboratory comparison (ILC) that tests transmission electron microscopy (TEM) protocols for image acquisition and analysis. Samples of CNCs were prepared on TEM grids in a single laboratory, and detailed data acquisition and analysis protocols were provided to participants. CNCs were imaged and the size of individual particles was analyzed in 10 participating laboratories that represent a cross section of academic, industrial, and government laboratories with varying levels of experience with imaging CNCs. The data for each laboratory were fit to a skew normal distribution that accommodates the variability in central location and distribution width and asymmetries for the various datasets. Consensus values were obtained by modeling the variation between laboratories using a skew normal distribution. This approach gave consensus distributions with values for mean, standard deviation, and shape factor of 95.8, 38.2, and 6.3 nm for length and 7.7, 2.2, and 2.9 nm for width, respectively. Comparison of the degree of overlap between distributions for individual laboratories indicates that differences in imaging resolution contribute to the variation in measured widths. We conclude that the selection of individual CNCs for analysis and the variability in CNC agglomeration and staining are the main factors that lead to variations in measured length and width between laboratories.

Cellulose nanocrystals (CNCs) are emerging nanomaterials derived from cellulose, the world's most abundant biopolymer.[1,2] Their large-scale production from a renewable resource, novel properties, and anticipated minimal toxicity make them an attractive candidate for a range of applications, some of which are nearing commercial success.[3−6] Application areas include additives for nanocomposites, thin films, rheology modifiers, and biomedical products. CNCs are produced from a number of cellulosic biomass sources, including trees and annual plants, bacteria, and marine organisms. They are nanorods with a typical aspect ratio of ≈15 (for wood pulp CNCs), a high crystalline cellulose content, high mechanical strength, and a low coefficient of thermal expansion. Most CNC production methods generate negatively charged groups on the particle surface, which provide colloidally stable dispersions and sites for further functionalization. Development of applications for this novel nanomaterial requires reliable characterization protocols that can be used to ensure reproducible production of the material from various biomass

Received: June 30, 2020
Accepted: August 31, 2020
Published: August 31, 2020

https://dx.doi.org/10.1021/acs.analchem.0c02805
Anal. Chem. 2020, 92, 13434−13442

sources and numerous producers. Validated characterization methods and reference materials are also necessary for studies aimed at ensuring the safe use of these materials.[7]

Key properties that must be assessed for CNCs include size and shape, crystallinity, and surface functional groups. It is challenging to measure CNC particle size distributions due to their irregular rod-shaped structure, broad size distributions, and strong tendency to agglomerate and aggregate. This is in contrast to well-behaved, spherical nanoparticles with narrow monomodal size distributions. Both transmission electron microscopy (TEM) and atomic force microscopy (AFM) have been employed by the CNC community for particle size measurements, although a standard approach for sample preparation, imaging, and image analysis is still lacking.[8−13] We report here the results of an interlaboratory comparison (ILC) conducted under the auspices of the Versailles Project on Advanced Materials and Standards (VAMAS) Technical Working Area 34 (Nanoparticle Populations). The objective was to assess the performance of protocols for TEM and AFM imaging of CNCs and subsequent particle size analysis. To reduce the impact of sample preparation on variability of specimens for imaging, the ILC used a National Research Council Canada (NRCC) reference material, CNCD-1, with samples prepared on substrates by the piloting laboratory. CNCD-1 was produced by sulfuric acid hydrolysis of softwood pulp, followed by neutralization with NaOH and spray drying and has been extensively characterized.[14] The results of this study will provide the prenormative data necessary for the development of a technical specification on measurement of CNC particle size distribution at ISO/TC 229 (Nanotechnologies). This paper focuses on a summary of the TEM results.

Transmission electron microscopy is generally considered the most reliable method for obtaining particle size distributions for nanomaterials. Most studies that have developed and validated TEM measurement protocols have employed gold, silica, or polystyrene nanoparticle reference materials.[15−17] These studies have been supported through international ILCs that allow one to assess measurement uncertainty and comparability across multiple laboratories. Nevertheless, these studies have utilized approximately spherical nanoparticles with low polydispersity and good TEM contrast and are not immediately adaptable to more complex "real-life" nanomaterials such as those produced industrially. One recent study has begun to address this complexity using a combination of particle counting, fractionation, and spectroscopy methods to evaluate the size distribution for a series of industrial nanomaterials with complex shapes and significant polydispersity; the results were compared to those obtained for well-defined spherical and monodisperse quality control samples.[18] It was concluded that a tiered approach using methods such as dynamic light scattering (DLS) for an initial screen and TEM for more detailed studies was appropriate for particle sizing. The issues associated with TEM measurements for nanomaterials with more complex shapes and strong agglomeration/aggregation have also recently been examined in a series of ILCs for gold nanorods, titanium dioxide nanoparticles, and carbon black.[19−21] These studies focused on a detailed assessment of image analysis methods for measurement of particle size distributions and provided a full uncertainty analysis, an essential feature to test for batch-to-batch similarity of materials or compare different CNC sources or preparation methods. They also provided the basis for publication of an ISO standard on TEM measurements of nanoparticles.[22]

Although the TEM protocols mentioned above provide a good basis for addressing some of the issues encountered for polydisperse and nonspherical nanomaterials, there are additional factors that require consideration for CNCs. Their shape is considerably less regular than that of the gold nanorods studied earlier; their TEM contrast, even after staining, makes it more difficult to distinguish CNCs from background; and the level of agglomeration is high, similar to the aggregates observed for TiO_2 or carbon black. These issues motivated this ILC, in which we focus on validating a measurement and analysis protocol that can be used to obtain CNC particle size distributions and assess uncertainty of the measurements. TEM particle size data from 10 participating laboratories were modeled using skew normal distributions for the dispersion of the measurement results provided by each laboratory as well as the dispersion that is observed between the laboratories.

EXPERIMENTAL SECTION

Sample Preparation. An NRCC-certified reference material, CNCD-1,[23] was dispersed by ultrasonication to give a 2% mass fraction CNC suspension that was deposited on plasma-treated carbon-coated copper grids and stained with uranyl acetate. A previously reported procedure[14,24] was optimized as outlined in the Supporting Information. ILC samples were prepared from a single CNC suspension on three separate days over an 11-day period to ensure that each laboratory received the sample on prearranged (convenient) date. One sample from each day was checked by TEM prior to shipping the samples, and DLS was used to verify that the suspension had not changed. Samples were sealed in a nitrogen glovebox prior to shipping. No change in image quality was observed over a 5-week storage period for samples of CNCs deposited on the TEM grid.

Participating Laboratories. The participating institutions were from Asia, Europe, and North America. These included three universities, six government laboratories, and one industrial laboratory. Not all laboratories had prior experience with imaging CNCs. Two samples of CNCs on carbon-coated copper grids were sent to each participant; the second sample was a backup. Participants were asked to image the samples within 2 weeks of receipt. Of the original 11 participants (randomly assigned a code, T#), 10 completed the ILC and returned datasets.

Image Acquisition and Analysis Protocol. The protocol requested the following operating conditions: (1) operating voltage between 80 and 300 kV; (2) ≈30 000 magnification such that the resolution is ≤0.3 nm/pixel; (3) calibration and lens normalization at the magnification used for CNC imaging; (4) acquisition of larger-scale images (e.g., 2 μm × 2 μm or larger) in multiple grid locations to locate suitable areas for higher-magnification images; and (5) collection of a sufficient number of images from multiple areas of the grid to analyze a minimum of 500 individual particles. Image analysis using a custom ImageJ macro was recommended, but participants had the option to use other software as long as the guidelines for particle selection were used. The ImageJ macro allows for automatic sequential opening of a set of images and manual measurement of length and width cross sections and saves the data and annotated images with the line profiles for analyzed CNCs. The criteria for selection of individual CNCs are provided in the Supporting Information.

https://dx.doi.org/10.1021/acs.analchem.0c02805
Anal. Chem. 2020, 92, 13434−13442

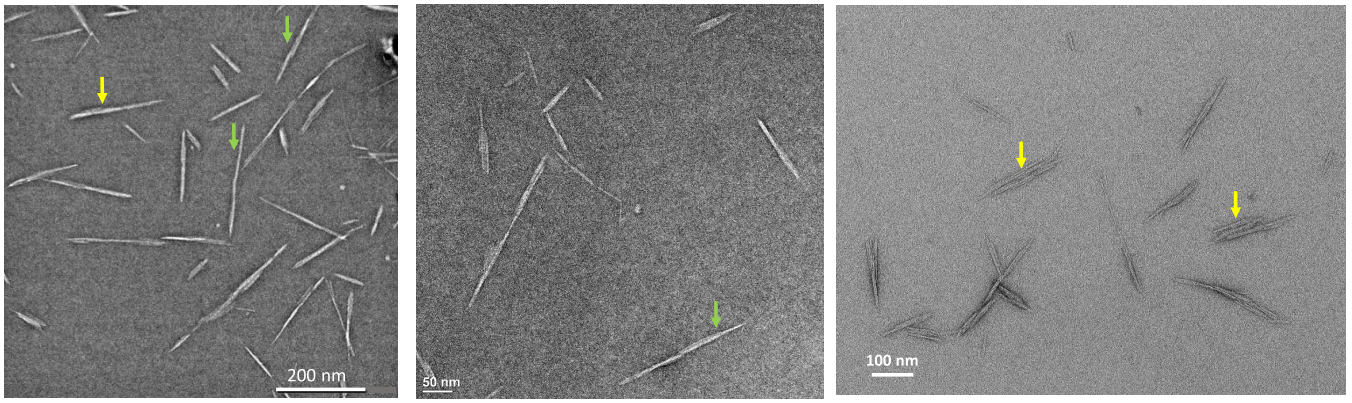

Figure 1. Representative TEM images from labs T3 (left), T6 (center), and T9 (right). The arrows mark features that are discussed in the text.

Data Analysis. Origin Pro 2019 was used for descriptive statistics and statistical comparison of datasets using the nonparametric two-sample Kolmogorov−Smirnov (K−S) test (e.g., length for lab 1 and lab 2). More complex data analysis and visualization were performed in R (free software environment for statistical computing and graphics). Skew normal model fitting was performed using Markov Chain Monte Carlo methods using STAN (a probabilistic programming language for statistical inference written in C++). The skew normal distribution differs from normal and lognormal distributions by the presence of an additional shape factor that allows for variable levels of skewness. Fitting was done using the individual data points, not the binned data shown in histograms. The overlap index used to compare particle size distributions was calculated by integrating the areas under curves using the standard numerical facilities of R.

RESULTS AND DISCUSSION

Tests of Image Analysis Protocols. The first phase of the ILC focused on testing ImageJ analysis methods. Three possible methods were considered. The first method was based on prior work in the piloting laboratory that used a semiautomated ImageJ macro to measure length and width manually for each particle.[14,24] Two other methods that were employed in recent TEM ILCs that analyzed gold nanorods and (aggregated) titanium dioxide were evaluated.[20,21] The contrast of stained CNCs against the substrate background was inadequate to utilize the automated approach based on thresholding that was employed for gold nanoparticles.[20] The method from the titanium dioxide ILC used the manual polygon outlining tool in ImageJ.[21] This manual outlining approach provides particle length and width (as maximum and minimum Feret, respectively) and other potentially useful parameters such as area and perimeter. Use of the polygon outlining tool gave length values in good agreement with the pilot laboratory's semiautomated ImageJ macro. However, the outlining tool consistently overestimated width compared to manual measurement using the semiautomated ImageJ macro. We hypothesize that the irregular tapered shape of the CNCs is incompatible with the minimum Feret measurement of the minimum distance between the two parallel tangents touching the particle outline. Therefore, the manual method using the semiautomated ImageJ macro to keep track of measurement data was adopted and further optimized for this ILC.

A set of images was provided to ILC participants to test the image analysis protocol. The images were a subset of those collected for one sample as part of the characterization of the NRCC-certified reference material, CNCD-1.[14] Six datasets were analyzed: the original CNCD-1 data for these images plus data from four laboratories, one of which submitted data from two analysts. Comparison of the results indicated that participants interpreted the image analysis protocol instructions differently. This was evident from the number of CNCs analyzed, which varied from 128 to 440. In one case, Olympus automated software was used for automated analysis (Lab 4). The box plots summarizing each dataset are shown in Figure S1 and demonstrate significant variability in the data. The means for length and width ranged from 71 to 105 nm and 7.0 to 10.0 nm, respectively (Table S1). K−S analysis indicated that all but two of the 15 possible pairs of datasets were significantly different for both length and width; the labs with no significant difference were different for the two measurands (Table S1).

Based on these observations and the feedback from participants, the image analysis protocol was modified to provide more detailed instructions for the selection of analyzable CNCs. Images with examples of analyzable CNCs and CNCs that should be excluded from size analysis were also provided as an Annex to the protocol (see Figures S2, S3, and S4). The improved protocol was used for CNC size analysis in the second phase of the ILC.

Initial Survey of TEM Results. Results were submitted from 10 participating laboratories; each participant submitted raw data (images), processed images with analyzed particles numbered, tables of length and width for each particle analyzed, length and width histograms, and a table with data acquisition and analysis information. The instruments, operating parameters, calibration, analysis software, and number of particles analyzed for each laboratory are summarized in Table S2. The resolution varied from ≈0.2 to 0.46 nm/pixel, with most labs collecting data at a resolution that was ≤20% larger than the recommended value of ≤0.3 nm/pixel. Lab 1 collected images using two magnifications; a K−S test indicated that there was no significant difference between the two datasets, so they were pooled for further analysis. In several cases, participants were asked to verify that the reported calibration was still valid. Most participants (9 of 10) reported data for 500 or more analyzed CNCs as requested; the largest dataset had 1179 particles and the smallest had 323 particles. The relatively small number of individual CNCs/image (typically 5 to 12 CNCs per μm^2) meant that all labs collected more than 50 images, making it

https://dx.doi.org/10.1021/acs.analchem.0c02805
Anal. Chem. 2020, 92, 13434−13442

impractical to compare intralaboratory repeatability on an image-by-image basis.

Representative images from three laboratories are shown in Figure 1. These images illustrate the variations in contrast and the significant agglomeration of CNCs that is typically observed, even at a low CNC density. See, for example, the arrows that highlight small clusters of laterally agglomerated CNCs in the T9 image. The number of features assigned to clustered CNCs is typically similar to or larger than the number of individual particles. The images from T3 and T6 have several irregularly shaped features that appear to be end-to-end CNCs (green arrows) and laterally agglomerated CNCs (yellow arrow). Note that such features may be counted in some cases but not others, depending on the image contrast and resolution and the analyst bias. Box plots of the length and width data for each laboratory are shown in Figure S5, and individual histograms for length, width, and aspect ratio for each laboratory are provided in Figures S6−S8, respectively. In several cases, examination of the box plots showed a few data points that suggested errors in reported data; this was verified by examining the image files and consulting the participant as to whether the data point(s) should be removed or corrected.

The results in Figures S5−S8 show qualitatively that the maximum position, shape, and width of the distributions vary from one dataset to the next for both length and width. The variability between laboratories is somewhat lower for aspect ratio, compared to length and width. Operator bias when deciding whether irregular features (such as those noted in Figure 1) are single CNCs contribute to this variability

Particle Size Distributions. Statistical modeling of interlaboratory results requires a selection of adequate probability density functions that describe the data at hand. Microscopy size measurements for CNCs typically provide data in the form of histograms and calculate the mean and the standard deviation as a measure of the distribution width, with the implicit assumption that the distributions fit a normal model. In several cases, the data have been shown to provide reasonable fits to a lognormal distribution.[25−28] Recent ILC studies of other nanomaterials have tested various distribution models in an attempt to better represent the overall central location and breadth/shape of the distributions. For example, the titanium dioxide ILC compared normal, lognormal, and Weibull distributions[21] whereas a recent comparison of electron microscopy and inductively coupled plasma-mass spectrometry (ICP-MS) data for gold nanoparticles employed mixtures of Gaussian distributions to model the complex shapes of the particle size distributions.[29] Others have adopted different statistical models for this purpose, for example by employing a (discrete) multinomial distribution.[30] Model selection has so far been largely empirical; furthermore, the CNC extraction method differs from bottom-up synthetic methods for metal or metal oxide nanoparticles, so there is no reason to anticipate that the same size distribution model will apply.

We have evaluated the particle size distributions against more than 50 continuous probability distributions using the tools implemented in the R package GAMLSS.[31] Probability density functions were fitted to data using the maximum likelihood method and ranked by the quality of each model as measured by the Bayesian Information Criterion (BIC). Several distributions produced a reasonable fit for our datasets, the simplest of which are the lognormal and skew normal distributions. Figure 2 shows the comparison of four statistical

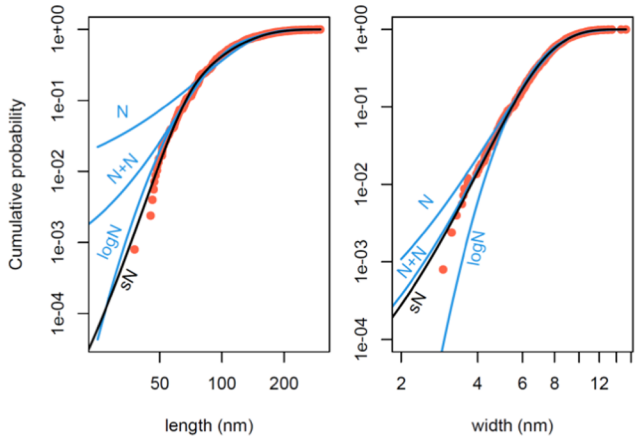

Figure 2. Log−log cumulative probability plots for CNC length and width for laboratory T1 with fits of normal (N), lognormal (logN), skew normal (sN), and two-mixture normal (N + N) distributions. The sN distribution provides a better fit than the other three models for both datasets.

models applied to the same datasets. These models are of varied complexity ranging from two parameters (normal or lognormal distributions) to three parameters (skew normal) to five parameters (two-mixture normal).

While one can always find a complex distribution that best fits a particular dataset, the results indicate that the skew normal distribution strikes a balance of being a model that is simple (three parameters), flexible (allows positive and negative skew), and fits the data very well. The skew normal distribution reduces to the normal distribution for datasets that show no asymmetry. Therefore, it is applicable to datasets that fit either a normal or lognormal distribution; the use of a single distribution facilitates comparison between datasets from different laboratories and the development of a consensus distribution, as explained in the following section.

The skew normal distribution (sN) is relatively new[32] and has been used to model grain-size distributions[33] among other applications.[34] Its probability density is derived by multiplying the normal distribution by the standard error function. The skew normal distribution has three parameters: location (μ), scale (σ, a measure of distribution width), and shape (α, a measure of distribution skew or asymmetry). Note that several parametrizations have been introduced to improve its mathematical performance (such as numerical stability or sampling efficiency).

The fitting was performed with the Markov Chain Monte Carlo method using STAN (a probabilistic programming language for statistical inference) and R. The facilities to construct and fit skew normal Bayesian models have been developed in the R package brms.[35] As an example, the following general syntax can be utilized to perform Bayesian fitting of the skew normal distribution

$$\text{brm(length} \sim 1, \text{ data, family} = \text{skew\_normal)} \quad (1)$$

Fits to a skew normal distribution for TEM length and width are shown for several representative datasets in Figure 3; all datasets are shown in Figures S6−S8. Table 1 summarizes mean, scale (as standard deviation), and skew normal shape parameters for length, width, and aspect ratio for each laboratory. Overall, the length distributions are broader (based on the relative standard deviations of their skew normal distributions) than the width distributions and show

https://dx.doi.org/10.1021/acs.analchem.0c02805
Anal. Chem. 2020, 92, 13434−13442

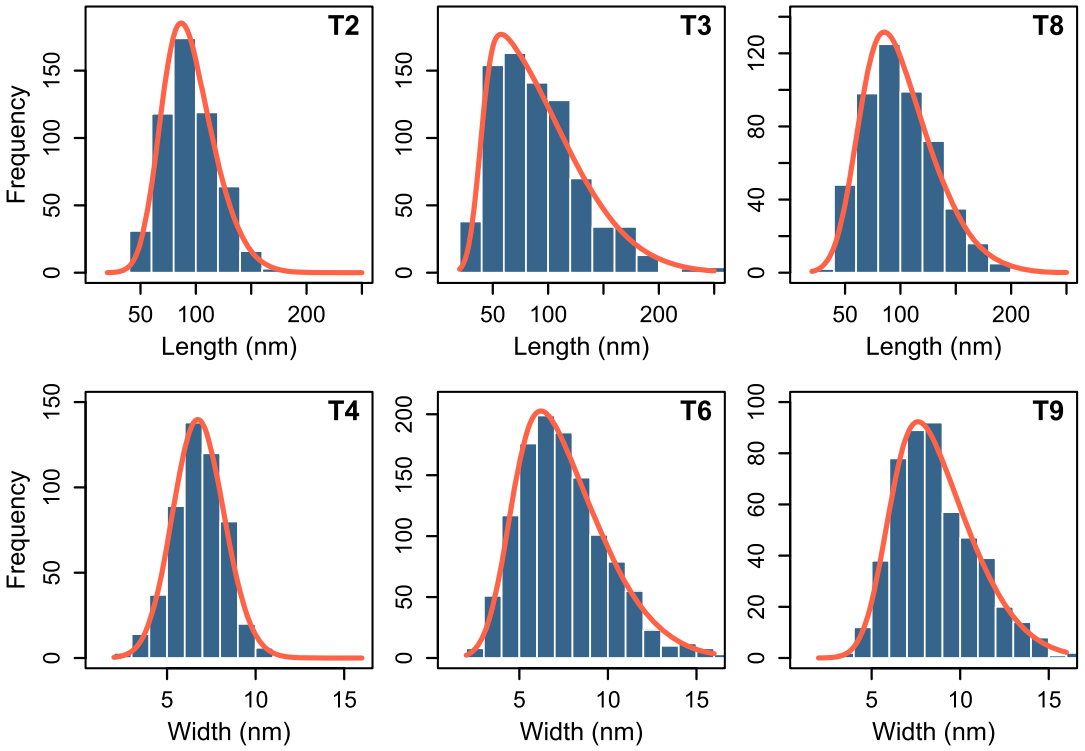

Figure 3. Representative datasets showing TEM histograms for length (top row) and width (bottom row) and a skew normal fit for the particle size distribution. Datasets were selected to show the range of distribution widths and shapes.

Table 1. Summary of Skew Normal Fit Parameters for Individual Lab Data and the Consensus Distribution for Length, Width, and Aspect Ratio Measurements by TEM

	length			width			aspect ratio		
laboratory	mean (nm)	std. dev. (nm)	sN shape, α	mean (nm)	std. dev. (nm)	sN shape, α	mean	std. dev.	sN shape, α
T1	116.6	44.5	6.6	7.8	1.9	1.5	15.7	6.4	9.5
T2	94.5	23.9	2.5	8.0	1.9	1.6	12.6	4.1	5.9
T3	91.9	41.1	8.0	7.5	2.1	4.0	12.9	5.4	6.9
T4	83.8	18.4	2.2	6.8	1.6	0.0	12.9	3.8	3.7
T5	86.4	35.8	6.7	8.0	1.6	2.8	11.1	4.8	8.2
T6	77.8	35.2	8.4	7.5	2.5	3.7	11.1	5.0	13.2
T7	87.6	35.6	6.1	6.9	1.9	3.5	13.5	5.8	9.7
T8	99.9	33.0	3.2	6.5	1.7	2.9	16.3	6.6	6.4
T9	102.8	43.3	8.8	8.7	2.3	3.2	13.0	5.9	9.0
T11	110.2	54.7	9.3	8.6	2.9	3.7	13.8	6.5	7.6
consensus value (standard uncertainty)	95.8 (0.4)	39.0 (0.3)	4.8 (0.2)	7.65 (0.02)	2.20 (0.02)	2.8 (0.1)	13.3 (0.06)	5.69 (0.05)	6.4 (0.3)
dispersion, t (standard uncertainty)	12.3 (0.5)			0.78 (0.03)			1.8 (0.1)		

larger variability between laboratories. The fitted skew normal distribution shape factors show a rough correlation with the scale/mean ratio for both length and width.

Consensus Distribution, Parameters, and Uncertainty. Data reduction from interlaboratory studies can be conducted in several ways. An approach that makes the fewest modeling assumptions is to pool all of the results together. Alternatively, one can establish a statistical model for individual laboratory results and the dispersion between the laboratories. The latter is formally known as the hierarchical random effects model. The general principles of applying a random effects model to interlaboratory studies have been outlined by Toman and Possolo[36] and Koepke et al.[37] More recently, similar models have been extended to deal with data exhibiting asymmetric tendencies.[38]

The statistical model of our ILC study follows the general principles of Montoro Bustos et al.[29] (pooling all results) with the exception of using a skew normal distribution to model the particle size distribution, rather than mixtures of Gaussian distributions. The skew normal consensus distribution was obtained by pooling the skew normal distributions representing the individual laboratory results. An equal number of random samples (N = 1000) was drawn from each of the skew normal distributions and placed into the pool. The statistical model of the entire ILC study (for each measurand) is therefore summarized by three parameters for each laboratory along with three additional parameters describing the

https://dx.doi.org/10.1021/acs.analchem.0c02805
Anal. Chem. 2020, 92, 13434−13442

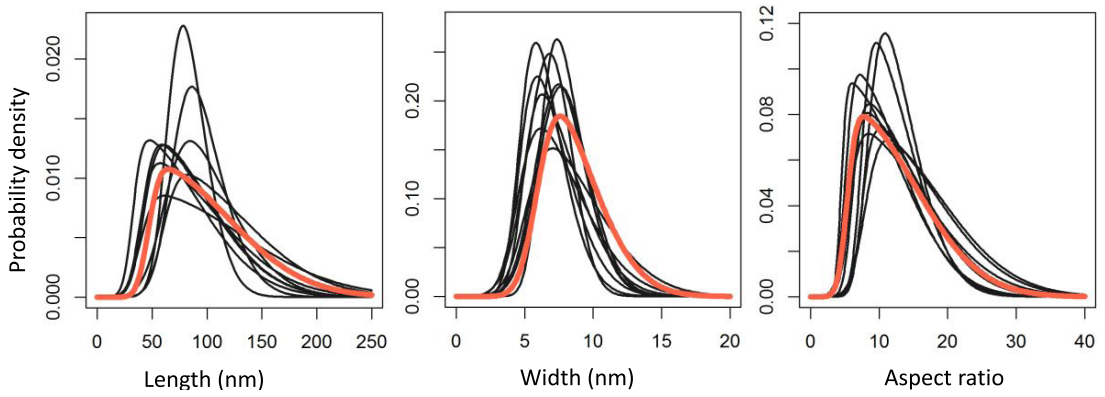

Figure 4. Skew normal probability densities describing the individual laboratory results (black lines) and the corresponding consensus distribution (orange line).

distribution of consensus values, the grand mean, scale, and shape.

The TEM data contain a total of 6168 observations from 10 laboratories for each of the measurands (width, length, and aspect ratio), and the fitting results for each laboratory and the consensus distribution are summarized in Figure 4. The final consensus data for length, width, and aspect ratio and the associated uncertainties are summarized in Table 1. The uncertainties are obtained as a direct output of fitting to the skew normal model. The dispersion between the mean laboratory results (t) is also provided as a measure of variability between the laboratories. The t values are all substantially larger than their uncertainties, which is indicative of significant spread in the datasets, as illustrated qualitatively by the histograms, box plots, and fitted parameters in Table 1. The dispersion value allows predictive assessment of how close the individual laboratory means should be to the consensus value.

Data Comparisons. The variability in skew normal distributions for the individual laboratories was examined using an overlap index which is defined as the relative common area between two distributions.[39] This is shown graphically in Figure 5, which provides the degree of overlap between individual datasets for both length and width. The mean, scale and shape parameters, and degree of overlap (Figure 5) can be used to test for correlations with changes in the experimental parameters used by the participating laboratories (Table S2). For width, three datasets have means that are smaller than 7 nm (T4, T7, and T8, Table 1) and all are measured at the best microscope resolution (0.20, 0.22, and 0.25 nm/pixel; Table S2). These three datasets have narrower particle width distributions as measured by the scale parameter, and two (T4 and T8) have the lowest average overlap (estimated as the average of the overlap with all other datasets, Figure 5) with other datasets. Overall, the results suggest that a resolution of 0.2 nm/pixel would give a more accurate estimate of width. However, there is a trade-off since that would generally require collection and analysis of a larger number of images to obtain the desired number of single particles for size analysis. By contrast, the dataset measured at the lowest resolution (T2, 0.46 nm/pixel) has a mean and scale that are close to the consensus values, which indicates that factors other than the resolution contribute to differences between laboratories. There is no apparent correlation with the number of CNCs analyzed, as the datasets with the highest (T6) and lowest (T5) N values have mean width and scale values that are close

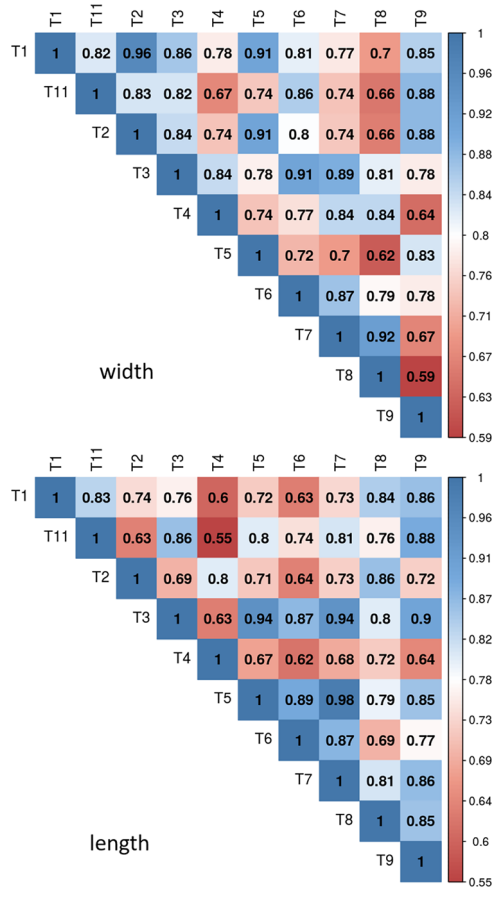

Figure 5. Degree of overlap (overlap index; relative common area between the two distributions) between datasets for width and length distributions.

to the overall consensus values (and used similar imaging resolutions) and an intermediate degree of overlap with other datasets. For pairwise comparisons (Figure 5), T8 and T9 have the lowest overlap of all pairs (0.59) followed by T8 and T5 (0.62). The low overlap reflects relatively large differences in both scale and mean for these two datasets.

The length overlap index graphic in Figure 5 indicates that the pairs of labs with the lowest overlap are T11/T4 (0.55) and T4/T1 (0.6); these variations are due to large differences in mean length and for the T4/T1 pair the largest difference in distribution width (scales of ≈18 and ≈55 nm for T4 and T1,

https://dx.doi.org/10.1021/acs.analchem.0c02805
Anal. Chem. 2020, 92, 13434−13442

respectively). The two datasets that show the lowest degree of overlap with other laboratories (T4 and T2) have the smallest scale factors (18 and 24 nm), similar to the observations for width above; the small scale factor is mainly due to the absence of longer CNCs, as illustrated in Figure 1. These datasets were measured using different resolutions (0.46 and 0.22 nm/pixel, Table S2), consistent with the expectation that particle length is insensitive to changes in resolution. Interestingly, these two labs have mean lengths that are close to the overall consensus value. The degree of overlap for length is lowest for the T4/T11 pair (0.55) and highest for the T5/T7 pair (0.98), which have almost the same mean and scale parameters. The datasets with the largest difference in the number of CNCs analyzed (323 and 1179 CNCs for T5 and T6, respectively) have similar scales and smaller means than the consensus value, providing little evidence that the number of CNCs analyzed has a major effect over the range covered here.

To test whether datasets with <500 analyzed CNCs yield repeatable results for a specific laboratory, smaller data subsets were compared for the two laboratories with the largest number of analyzed CNCs (T3 and T6). K−S tests showed that particle width distributions for datasets of ≈280 CNCs were different for both labs. By contrast, the length distributions for the data subsets were different for T3 but not for T6. The number of points needed to obtain stable size measurements was also examined by plotting the cumulative mean as a function of the number of analyzed particles, as shown in Figure S9 for several datasets. This shows that the mean length stabilizes with 200−300 analyzed particles in some cases but not others. The TEM width variations are similar to a one-pixel error for some datasets (pixel sizes of 0.2−0.4 nm for the labs shown); however, in other cases, the width continues to vary with an increasing number of analyzed particles. Although more detailed studies are required to make a definitive conclusion, we hypothesize that variations in CNC agglomeration and staining for different grid areas may account for these results. This issue makes it difficult to establish an optimal number of analyzed particles without verifying whether a stable particle length and width are obtained. A comparison of length and width skew normal fit parameters indicates that the magnitude of the mean and scale parameters follow a similar pattern for individual laboratories. Dataset T11 has the largest scale factor and the second largest mean for both length and width. This does not appear to correlate with the resolution used or the number of CNCs analyzed. Although the T11 dataset was obtained using different analysis software, visual inspection of analyzed images provides no indication that the selection of analyzable CNCs is different for this laboratory. The mean and scale for dataset T9 are also among the largest for both length and width and T4 has the smallest scale and second smallest mean for length and the second smallest mean and scale for width. Based on the initial image analysis tests, it can be concluded that the selection of individual CNCs for analysis is a significant contributor to differences between laboratories.

The consensus values can be compared to the data reported for CNCD-1, which was characterized by TEM in two laboratories. The reported values for mean (standard deviation) were 87 (35) nm and 7.3 (1.8) for length and width, respectively, for the combined data from the two laboratories.[14] These values fall within the range of results obtained from the 10 ILC laboratories (Table 1); however, the ILC data indicate that a mean value of ≈96 nm provides a better estimate of the CNC length for CNCD-1 than the previously reported value of 87 nm.[23] It should also be noted that the original data were not obtained by fitting to a skew normal distribution, which is anticipated to lead to a small (1−2 nm) difference in values. The previous study examined five independently prepared samples, all of which were analyzed by a single analyst;[14] the variability in length was lower than that observed in the ILC, although the width variability was similar. The latter indicates that variations in length for the ILC include contributions from sample-to sample variations and differences between laboratories/analysts.

As noted above, analyst bias/subjectivity and sample heterogeneity are the main sources of ILC variability. The subjectivity in choice of analyzable CNCs can in principle be reduced by use of automated image analysis methods that are currently being developed. Although significant effort was made to optimize the CNC deposition and staining method used to prepare samples for this ILC, agglomeration and uneven staining remain an issue. Recent work has demonstrated that fractionation of CNCs using asymmetric flow field flow fractionation can significantly reduce the level of CNC agglomerates, yielding samples that almost eliminate clusters as assessed by AFM imaging.[40] The fractionated samples show some improvement in dispersion on TEM grids, although there are significantly more clusters than observed in samples deposited for AFM.

CONCLUSIONS

The ILC data obtained from 10 laboratories show variability in the central location, width, and asymmetry of the measured particle size distributions for length and width. To make quantitative comparisons between individual datasets and facilitate development of consensus values, we have employed an approach wherein each dataset is fit to a skew normal distribution that yields three parameters: mean as a measure of the central location, standard deviation as a measure of the distribution scale/width, and a shape parameter as a measure of the distribution asymmetry. This approach has the advantage of using a single distribution that can adequately deal with the variability in the data while introducing only one new fit parameter compared to the two-parameter distributions, such as normal or lognormal, that have frequently been employed for fitting particle size distributions. This approach also has fewer parameters than fits to sums of distributions.

Consensus values are obtained from the individual datasets by modeling the variation between laboratories using a skew normal distribution. This gives values for the consensus distribution for mean, standard deviation, and shape of 95.8, 38.2, and 6.3 nm, respectively, for length and 7.7, 2.2 and 2.9 nm, respectively, for width, with uncertainties as listed in Table 1. Attempts to correlate the lab-to-lab variability with differences between experimental conditions for data acquisition and analysis indicated that a higher magnification for image acquisition yielded particle width distributions with smaller mean and standard deviation values. One can conclude that a resolution of <0.3 nm/pixel would be preferable for CNC imaging, although collection of additional images may be necessary to obtain the required number of particles for analysis and may lead to rejection of a larger fraction of long particles. However, the use of a smaller pixel size did not appear to be a factor in determining the measured differences in length. Overall, we conclude that the selection of individual particles for image analysis is one of the larger contributors to

https://dx.doi.org/10.1021/acs.analchem.0c02805
Anal. Chem. 2020, 92, 13434−13442

differences between laboratories, even after implementing an improved analysis protocol based on the results of the image analysis tests in phase 1. Variability in CNC agglomeration/aggregation and staining[11] is another important factor; this is difficult to control even after optimizing the protocol and preparing all samples in the piloting laboratory.

Finally, we note that the AFM imaging results obtained during this ILC will be reported elsewhere. A final comparison of size measurements from the two microscopy methods will provide a useful assessment of methods for image acquisition and analysis procedures for CNCs. It will also give insight into the agreement between laboratories and the approaches necessary to make comparisons between different CNC sources and their characterization in different laboratories.

■ ASSOCIATED CONTENT

Supporting Information

The Supporting Information is available free of charge at https://pubs.acs.org/doi/10.1021/acs.analchem.0c02805.

Additional experimental details and tables and figures summarizing the image analysis protocol and tests and histograms and fits for all datasets (PDF)

■ AUTHOR INFORMATION

Corresponding Author

Linda J. Johnston − *National Research Council Canada, Ottawa, Ontario K1A 0R6, Canada;* orcid.org/0000-0002-9136-4920; Email: Linda.Johnston@nrc-cnrc.gc.ca

Authors

Juris Meija − *National Research Council Canada, Ottawa, Ontario K1A 0R6, Canada*

Michael Bushell − *National Research Council Canada, Ottawa, Ontario K1A 0R6, Canada*

Martin Couillard − *National Research Council Canada, Ottawa, Ontario K1A 0R6, Canada*

Stephanie Beck − *FPInnovations, Pointe-Claire, Quebec H9R 3J9, Canada*

John Bonevich − *Materials Science and Engineering Division, National Institute of Standards and Technology, Gaithersburg, Maryland 20899, United States*

Kai Cui − *National Research Council Canada, Nanotechnology Research Centre, Edmonton, Alberta T6G 2M9, Canada*

Johan Foster − *Department of Materials Science and Engineering, Virginia Tech, Blacksburg, Virginia 24061, United States; Chemical and Biological Engineering, The University of British Columbia, Vancouver, British Columbia V6T 1Z3, Canada*

John Will − *Department of Materials Science and Engineering, Virginia Tech, Blacksburg, Virginia 24061, United States*

Douglas Fox − *Department of Chemistry, American University, Washington, District of Columbia 20016, United States*

Whirang Cho − *Department of Chemistry, American University, Washington, District of Columbia 20016, United States*

Markus Heidelmann − *Interdisciplinary Center for Analytics on the Nanoscale, University of Duisburg-Essen, 47057 Duisburg, Germany*

Byong Chon Park − *Center for Nanocharacterization, Korea Research Institute of Standards and Science, Daejeon 34113, Republic of Korea*

Yun Chang Park − *Division of Measurement & Analysis, National Nanofab Center, Daejeon 34141, Republic of Korea*

Lingling Ren − *National Institute of Metrology, Beijing 100029, China*

Li Xu − *National Institute of Metrology, Beijing 100029, China*

Aleksandr B. Stefaniak − *National Institute for Occupational Safety and Health, Morgantown, West Virginia 26505, United States*

Alycia K. Knepp − *National Institute for Occupational Safety and Health, Morgantown, West Virginia 26505, United States*

Ralf Theissmann − *KRONOS INTERNATIONAL Inc., 51373 Leverkusen, Germany*

Horst Purwin − *KRONOS INTERNATIONAL Inc., 51373 Leverkusen, Germany*

Ziqiu Wang − *Electron Microscopy Laboratory, National Cancer Institute, Center for Cancer Research, Leidos Biomedical Research, Frederick National Laboratory, Frederick, Maryland 21702, United States*

Natalia de Val − *Electron Microscopy Laboratory, National Cancer Institute, Center for Cancer Research, Leidos Biomedical Research, Frederick National Laboratory, Frederick, Maryland 21702, United States*

Complete contact information is available at: https://pubs.acs.org/10.1021/acs.analchem.0c02805

Notes

Any mention of commercial products is for information only; it does not imply recommendation or endorsement by NIST. The authors declare no competing financial interest.

■ ACKNOWLEDGMENTS

Financial support from Natural Resources Canada for ongoing support of NRC's work on standardization of CNCs is gratefully acknowledged. The authors thank the following people for their input: Dr. Jeff Fagan, NIST, for useful advice while planning this ILC; Dr. Xiaohua Wu and Dr. Marek Malac, NRCC, for TEM assistance and advice; and Dr. Sylvain Gendron and Dr. Carole Fraschini (FPInnovations) for analysis and useful discussions.

■ REFERENCES

(1) Moon, R. J.; Martini, A.; Nairn, J.; Simonsen, J.; Youngblood, J. *Chem. Soc. Rev.* **2011**, *40*, 3941−3994.

(2) Klemm, D.; Kramer, F.; Moritz, S.; Lindstrom, T.; Ankerfors, M.; Gray, D.; Dorris, A. *Angew. Chem., Int. Ed.* **2011**, *50*, 5438−5466.

(3) Shatkin, J. A.; Wegner, T. H.; Bilek, E. M.; Cowie, J. *Tappi J.* **2014**, *13*, 9−16.

(4) Grishkewich, N.; Mohammed, N.; Tang, J.; Tam, C. *Curr. Opin. Colloid Interface Sci.* **2017**, *29*, 32−45.

(5) Mondal, S. *Carbohydr. Polym.* **2017**, *163*, 301−316.

(6) Mokhena, T. C.; John, M. J. *Cellulose* **2020**, *27*, 1149−1194.

(7) Shatkin, J. A.; Kim, B. *Environ. Sci.: Nano* **2015**, *2*, 477−499.

(8) Foster, E. J.; Moon, R. J.; Agarwal, U. P.; Bortner, M. J.; Bras, J.; Camarero-Espinosa, S.; Chen, K. J.; Clift, M. J. D.; Cranston, E. D.; Eichhorn, S. J.; Fox, D. M.; Hamad, W. Y.; Heux, L.; Jean, B.; Korey, M.; Nieh, W.; Ong, K. J.; Reid, M. S.; Renneckar, S.; Roberts, R.; Shatkin, J. A.; Simonsen, J.; Stinson-Bagby, K.; Wanasekara, N.; Youngblood, J. *Chem. Soc. Rev.* **2018**, *47*, 2609−2679.

(9) Kaushik, M.; Fraschini, C.; Chauve, G.; Putaux, J.-L.; Moores, A. Transmission Electron Microscopy for the Characterization of Cellulose Nanocrystals. In *The Transmission Electron Microscope - Theory and Applications*; Maaz, K., Ed.; Intech, 2015; pp 129−163.

(10) Ogawa, Y.; Putaux, J.-L. *Cellulose* **2019**, *26*, 17−34.

(11) Stinson-Bagby, K. L.; Roberts, R.; Foster, E. J. *Carbohydr. Polym.* **2018**, *186*, 429−438.

(12) Moon, R. J.; Pohler, T.; Tammelin, T. Microscopic Characterization of Nanofibers and Nanocrystals. In *Handbook of Green*

Materials; Oksman, K. et al., Ed.; World Scientific: Singapore, pp 2014; 159−180.
(13) Sacui, I. A.; Nieuwendaal, R. C.; Burnett, D. J.; Stranick, S. J.; Jorfi, M.; Weder, C.; Foster, J. E.; Olsson, R. T.; Gilman, J. W. *ACS Appl. Mater. Interfaces* **2014**, *6*, 6127−6138.
(14) Jakubek, Z. J.; Chen, M.; Couillard, M.; Leng, T.; Liu, L.; Zou, S.; Baxa, U.; Clogston, J. D.; Hamad, W. Y.; Johnston, L. J. *J. Nanopart. Res.* **2018**, *20*, No. 98.
(15) Rice, S. B.; Chan, C.; Brown, S. C.; Eschbach, P.; Han, L.; Esnor, D. S.; Stefaniak, A. B.; Bonevich, J.; Vladar, A. E.; Hight Walker, A. R.; Zheng, J.; Starnes, C.; Stromberg, A.; Ye, J.; Grulke, E. A. *Metrologia* **2013**, *50*, 663−678.
(16) De Temmerman, P.-J.; Lammertyn, J.; De Ketelare, B.; Kestens, V.; Roebben, G.; Verleysen, E.; Mast, J. *J. Nanopart. Res.* **2014**, *16*, No. 2177.
(17) Meli, F.; Klein, T.; Buhr, E.; Frase, C. G.; Gleber, G.; Krumrey, M.; Duta, A.; Duta, S.; Korpelainen, V.; Bellotti, R.; Picotto, G. B.; Boyd, R. D.; Cuenat, A. *Meas. Sci. Technol.* **2012**, *23*, No. 125005.
(18) Babick, F.; Mielke, J.; Wohlleben, W.; Weigel, S.; Hodoroaba, V.-D. *J. Nanopart. Res.* **2016**, *18*, No. 158.
(19) Grulke, E.; B. Rice, S.; Xiong, J.; Yamamoto, K.; Yoon, T. H.; Thomson, K.; Saffaripour, M.; Smallwood, G.; Lambert, J.; Stromberg, A.; Macy, R.; Briot, N.; Qian, D. *Carbon* **2018**, *130*, 822−833.
(20) Grulke, E. A.; Wu, X.; Ji, Y.; Buhr, E.; Yamamoto, K.; Song, N. W.; Stefaniak, A. B.; Schwegler-Berry, D.; Burchett, W. W.; Lambert, J.; Stromberg, A. J. *Metrologia* **2018**, *55*, 254−267.
(21) Grulke, E. A.; Yamamoto, K.; Kumagi, K.; Hausler, I.; Osterle, W.; Ortel, E.; Hodoroaba, V.-D.; Brown, S. C.; Chan, C.; Zheng, J.; Yamamoto, K.; Yashiki, K.; Song, N. W.; Kim, Y. H.; Stefaniak, A. B.; Schwegler-Berry, D.; Coleman, V. A.; Jamting, A. K.; Hermann, J.; Arakawa, T.; Burchett, W. W.; Lambert, J. W.; Stromberg, A. J. *Adv. Powder Technol.* **2017**, *28*, 1647−1659.
(22) ISO 21363:2020 Nanotechnologies - measurements of particle size and shape distributions by transmission electron microscopy.
(23) http://www.nrc.ca/crm.
(24) Brinkmann, A.; Chen, M.; Couillard, M.; Jakubek, Z. J.; Leng, T.; Johnston, L. J. *Langmuir* **2016**, *32*, 6105−6114.
(25) Elazzouzi-Hafraoui, S.; Nishiyama, Y.; Putaux, J.-L.; Heux, L.; Dubreuilf, F.; Rochas, C. *Biomacromolecules* **2008**, *9*, 57−65.
(26) Postek, M. T.; Vladar, A.; Dagata, J.; Farkas, N.; Ming, B.; Wagner, R.; Raman, A.; Moon, R. J.; Sabo, R.; Wegner, T. H.; Beecher, J. *Meas. Sci. Technol.* **2011**, *22*, No. 024005.
(27) Usov, I.; Nystrom, G.; Adamcik, J.; Handschin, S.; Schutz, C.; Fall, A.; Bergstrom, L.; Mezzenga, R. *Nat. Commun.* **2015**, *6*, No. 7564.
(28) Meng, Y.; Wu, Q.; Young, T. M.; Huang, B.; Wang, S.; Li, Y. *Polym. Compos.* **2017**, *38*, 2368−2377.
(29) Montoro Bustos, A. R.; Petersen, E. J.; Possolo, A.; Winchester, M. R. *Anal. Chem.* **2015**, *87*, 8809−8817.
(30) Petersen, E. J.; Montoro Bustos, A. R.; Toman, B.; Johnson, M. E.; Ellefson, M.; Caceres, G. C.; Neuer, A. L.; Chan, Q.; Kemling, J. W.; Mader, B.; Murphy, K.; Roesslein, M. *Environ. Sci.: Nano* **2019**, *6*, 2876−2896.
(31) Voncken, L.; Albers, C. J.; Timmerman, M. E. *Assessment* **2019**, *26*, 1329−1346.
(32) O'Hagan, A.; Leonard, T. *Biometrika* **1976**, *63*, 201−203.
(33) Yuan, R.; Zhang, C.; Wang, X.; Zhu, R. *Arabian J. Geosci.* **2018**, *11*, No. 695.
(34) Lin, T. I.; Lee, J. C. *Stat. Med.* **2008**, *27*, 1490−1507.
(35) Bürkner, P.-C. Brms: An R package for Bayesian multilevel models using stan. *J. Stat. Software* **2017**, *80*, , DOI: 10.18637/jss.v080.i01.
(36) Toman, B.; Possolo, A. *Accredit. Qual. Assur.* **2009**, *14*, 553−563.
(37) Koepke, A.; Lafarge, T.; Possolo, A.; Toman, B. *Metrologia* **2017**, *54*, S34−S62.
(38) Possolo, A.; Merkatas, C.; Bodnar, O. *Metrologia* **2019**, *56*, No. 045009.
(39) Pastore, M.; Calcagnì, A. *Front. Psychol.* **2019**, *10*, No. 1089.
(40) Chen, M.; Parot, J.; Mukherjee, A.; Couillard, M.; Zou, S.; Hackley, V. A.; Johnston, L. J. *Cellulose* **2020**, *27*, 2015−2028.

https://dx.doi.org/10.1021/acs.analchem.0c02805
Anal. Chem. 2020, 92, 13434−13442